Interplay between spin frustration and magnetism in the exactly solved two-leg mixed spin ladder*

Yan Qi(齐岩)[1,†], Song-Wei Lv(吕松玮)[1], An Du(杜安)[2], and Nai-sen Yu(于乃森)[1,‡]

[1] School of Physics and Materials Engineering, Dalian Nationalities University, Dalian 116600, China
[2] College of Sciences, Northeastern University, Shenyang 110819, China

(Received 21 May 2016; revised manuscript received 28 July 2016; published online 28 September 2016)

We study a mixed spin-(3/2, 1) ladder system with antiferromagnetic rung coupling and next-nearest-neighbor interaction. The exactly solved Ising-chain model is employed to investigate the ground-state properties and thermodynamics of the low-dimensional ladder system. Our results show that the competition between different exchange couplings brings in a large variety of ground states characterized by various values of normalized magnetization equal to 0, 1/5, 2/5, 3/5, 1. Moreover, an interesting double-peak structure is also detected in the thermal dependence of magnetic susceptibility and specific heat when the frustration comes into play. It is shown that the double-peak phenomenon at zero-field for the case of AF_2 ground-state arises from the very strong antiferromagnetic rung coupling, while other cases are attributed to the excitations induced by temperature and external field around the phase boundary.

Keywords: mixed-spin ladder, transfer-matrix method, exact solution, frustration

PACS: 75.10.Pq, 75.30.Kz, 75.40.Cx **DOI:** 10.1088/1674-1056/25/11/117501

1. Introduction

Low-dimensional spin systems with competing exchange interactions have received a great deal of attention in condensed matter physics.[1,2] Among various low-dimensional spin systems, frustrated magnetic ladders with different topologies of couplings offer an intriguing example to study exotic and complex phenomena such as high-temperature superconductivity, quantum phase transition, thermal conductivity, and many other interesting properties.[3–6] Theoretical and experimental investigations have shown that the main characters of spin ladders are largely determined by the number of legs. Ladders with an even number of legs have a finite spin gap between the singlet ground state and the magnetic excited states, while ladders with an odd number of legs exhibit a gapless spectrum and behave as single chains.[7]

However, most of the previous studies were focused on the ladder systems with uniform spin as the synthesized spin-ladder materials of that period basically contained one type of transition-metal magnetic ion.[8–10] In recent years, molecular magnets of ladder topology with mixed-spin structure have been experimentally realized, such as bimetallic compounds $MnCu(PbaOH)(H_2O)_3$ (pbaOH=2-hydroxy-1,3-propylenebisoxamato), $MnCu(pba)(H_2O)_3{\cdot}2H_2O$, and $NiCu(pba)(D_2O)_3{\cdot}2D_2O$ (pba = 1,3-propylenebis),[11,12] motivating the related theoretical work to be carried out. The two-leg mixed spin-(1,1/2) ladder is one of the most studied systems due to the simplicity of mixture and experimental realization in several compounds. The calculated results have indicated that an interplay between frustration and spin alternation can produce both classical and quantum ferrimagnetic orders in this system, as well as interesting magnetization-plateau behaviors.[13–15] A generic quantum Heisenberg spin model is usually used to explain these exotic findings, though this model proves to be very useful, it cannot be rigorously solved due to mathematical complexities caused by non-commutability of spin operators. Therefore, various approximation methods including spin-wave series, density-matrix renormalization group, and transfer-matrix renormalization group are adopted to study the thermodynamics and magnetism. Owing to this fact, a simplified version of the quantum Heisenberg model in which the spins are partially or completely replaced by the Ising-type ones is introduced.[16] It has been demonstrated that this simple Ising model is not only exactly soluble, but also displays good correspondence to the pure quantum model under certain conditions.[17–19] In this work, we will employ this simplified Ising-chain model to study the mixed-spin ladder system, which is consist of a spin-3/2 chain coupled with a spin-1 chain through the rung and diagonal exchange bonds. The mixed-spin structure of the two-leg ladder is illustrated in Fig. 1. The motivation for studying such a system is twofold. One is the fundamental curiosity closely linked with the underlying competing mechanism, and the other is the recent experimental achievements

*Project supported by the National Natural Science Foundation of China (Grant No. 11547236), the General Project of the Education Department of Liaoning Province, China (Grant No. L2015130), the Fundamental Research Funds for the Central Universities, China (Grant Nos. DC201501065 and DCPY2016014), and the Doctoral Starting-up Foundation of Dalian Nationalities University, China.

†Corresponding author. E-mail: qiyan@dlnu.edu.cn
‡Corresponding author. E-mail: naisenyu@163.com

© 2016 Chinese Physical Society and IOP Publishing Ltd

in ladder compounds.

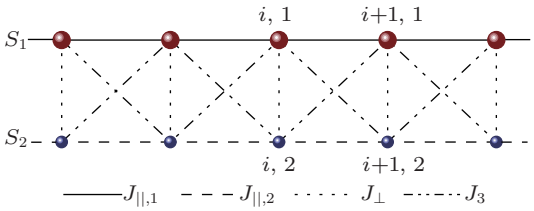


Fig. 1. (color online) Sketch of the two-leg mixed spin ladder. Large wine (small navy) circles denote $S_1 = 3/2$ ($S_2 = 1$) spin.

2. Model and method

The Hamiltonian of the exactly solved ladder model reads

$$\begin{aligned}\mathcal{H} = & \sum_i J_{||,1} S_{i,1} S_{i+1,1} + \sum_i J_{||,2} S_{i,2} S_{i+1,2} + \sum_i J_\perp S_{i,1} S_{i,2} \\ & + \sum_i J_3 (S_{i,1} S_{i+1,2} + S_{i+1,1} S_{i,2}) \\ & - H \sum_i (g_1 \mu_B S_{i,1} + g_2 \mu_B S_{i,2}), \end{aligned} \tag{1}$$

where $S_{i,1}$ ($S_{i,2}$) denotes the $S = 3/2$ ($S = 1$) spin at site i of one leg, $J_{||,1}$ ($J_{||,2}$) is the interaction between nearest-neighbor spins along the chain, $J_\perp$ is the vertical rung coupling between the two spin chains, J_3 is the diagonal exchange interaction between the second-neighbor spins, g_1 (g_2) is the Lande factor for spin-3/2 (spin-1), μ_B is the Bohr magneton, and H is the external magnetic field. In the following, we take $g_1\mu_B = g_2\mu_B = 1$ for simplicity.

For convenience, the total Hamiltonian can be rewritten as a sum of block Hamiltonians $\mathcal{H} = \sum_i \mathcal{H}_{i,i+1}$, where each Hamiltonian block contains all magnetic interaction terms

$$\begin{aligned}\mathcal{H}_{i,i+1} = & J_{||,1} S_{i,1} S_{i+1,1} + J_{||,2} S_{i,2} S_{i+1,2} \\ & + \frac{J_\perp}{2} (S_{i,1} S_{i,2} + S_{i+1,1} S_{i+1,2}) \\ & + J_3 (S_{i,1} S_{i+1,2} + S_{i+1,1} S_{i,2}) \\ & - \frac{H}{2} [(S_{i,1} + S_{i+1,1}) + (S_{i,2} + S_{i+1,2})]. \end{aligned} \tag{2}$$

It is noteworthy that Hamiltonian block $\mathcal{H}_{i,i+1}$ of the mixed-spin ladder model can be straightforwardly used to obtain all possible ground states and the corresponding energies. Meanwhile, it also implies the possibility of performing the transfer-matrix method to access the exact solution of any concerned thermodynamic property. According to the definition of the partition function, one obtains the following expression:

$$\mathcal{Z} = \mathrm{Tr} e^{-\beta \mathcal{H}}. \tag{3}$$

Here $\beta = 1/(k_B T)$, k_B is the Boltzmann's constant and set to be unity here, and T is the absolute temperature. By employing unitary transformation, $\mathcal{Z}$ can be further written as

$$\begin{aligned}\mathcal{Z} = & \mathrm{Tr} e^{-\beta \mathcal{H}} = \mathrm{Tr}(\boldsymbol{V}^{-1}\boldsymbol{P}\boldsymbol{V}\boldsymbol{V}^{-1}\boldsymbol{P}\boldsymbol{V}\cdots\boldsymbol{V}^{-1}\boldsymbol{P}\boldsymbol{V}) = \mathrm{Tr}\boldsymbol{\lambda}^N \\ = & \lambda_1^N + \lambda_2^N + \lambda_3^N + \cdots + \lambda_{12}^N, \end{aligned} \tag{4}$$

where $\boldsymbol{V}$ is a unitary matrix and satisfies the relation $\boldsymbol{V}^{-1}\boldsymbol{V} = \boldsymbol{I}$. $\boldsymbol{P}$ is the transfer-matrix with the matrix elements

$$P_{ln} = \langle S_{i,1}(l), S_{i,2}(l) | \exp(-\beta \mathcal{H}_{i,i+1}) | S_{i+1,1}(n), S_{i+1,2}(n) \rangle, \tag{5}$$

where l and n are dependent on the dimension of $\boldsymbol{P}$. Apparently, the dimension of $\boldsymbol{P}$ is determined by the number of states that the subsystem possesses. Here, $S_{i,1}$ takes the value of $\pm 3/2, \pm 1/2$, and $S_{i,2}$ takes the value of $0, \pm 1$, therefore $\boldsymbol{P}$ is a 12×12 matrix with twelve eigenvalues, and $l, n = 1, 2, \ldots, 12$. For clarity and convenience, λ_1 is assumed to be the largest eigenvalue in the following elaboration. If all the eigenvalues are nondegenerate and the largest one λ_1 is real, in the thermodynamic limit, the partition function is simply given by

$$\lim_{N\to\infty} \mathcal{Z} = \lambda_1^N, \tag{6}$$

and the corresponding free energy per block is

$$f = -k_B T \ln \lambda_1. \tag{7}$$

Once the free energy has been obtained, the physical quantities we focus on in terms of f can also be determined. According to quantum canonical ensemble theory, the thermodynamic average of an arbitrary quantity A is defined as $\langle A \rangle = \frac{1}{\mathcal{Z}} \mathrm{Tr}[A e^{(-\beta \mathcal{H})}]$. Then the average magnetization m, magnetic susceptibility χ, and magnetic specific C_m can be written in the following forms:

$$\begin{aligned} m = & \frac{1}{N} \Big\langle \sum_i \frac{(S_{i,1} + S_{i,2})}{2} \Big\rangle, \\ \chi_m = & \frac{1}{NT} \left(\Big\langle \Big[\sum_i \frac{(S_{i,1} + S_{i,2})}{2} \Big]^2 \Big\rangle - \Big\langle \sum_i \frac{(S_{i,1} + S_{i,2})}{2} \Big\rangle^2 \right), \\ C_m = & \frac{1}{NT^2} (\langle \mathcal{H}^2 \rangle - \langle \mathcal{H} \rangle^2). \end{aligned} \tag{8}$$

With further application of the transfer-matrix method, the final analytical expression for the average magnetization is obtained as

$$\begin{aligned} m = & \frac{1}{N} \Big\langle \sum_i \frac{(S_{i,1} + S_{i,2})}{2} \Big\rangle \\ = & \frac{1}{N} \frac{\mathrm{Tr}\Big[\sum_i \frac{(S_{i,1} + S_{i,2})}{2} e^{-\beta \mathcal{H}} \Big]}{\mathrm{Tr} e^{-\beta \mathcal{H}}} = S'_{11}, \end{aligned} \tag{9}$$

where $\boldsymbol{S}' = \boldsymbol{V}^{-1}\boldsymbol{S}\boldsymbol{V}$, and $\boldsymbol{S}$ is a diagonal matrix with diagonal elements

$$S_{ll} = \left\langle S_{i,1}(l), S_{i,2}(l) \middle| \frac{(S_{i,1} + S_{i,2})}{2} \middle| S_{i,1}(l), S_{i,2}(l) \right\rangle.$$

In the same way, we can obtain the final expressions of average magnetic susceptibility and magnetic specific heat as follows:

$$\chi_m = \frac{1}{NT} \left(\Big\langle \Big[\sum_i \frac{(S_{i,1} + S_{i,2})}{2} \Big]^2 \Big\rangle - \Big\langle \sum_i \frac{(S_{i,1} + S_{i,2})}{2} \Big\rangle^2 \right)$$

$$= \frac{1}{T}\sum_{k=2}^{12} S'_{1k}S'_{k1}\frac{1}{1-\lambda_k/\lambda_1}, \tag{10}$$

$$C_{\rm m} = \frac{1}{NT^2}(\langle\mathcal{H}^2\rangle - \langle\mathcal{H}\rangle^2)$$
$$= \frac{1}{T^2}\Big(\frac{(\boldsymbol{B}'\boldsymbol{B}')_{11}}{\lambda_1} - \frac{(\boldsymbol{D}'\boldsymbol{D}')_{11}}{\lambda_1^2}$$
$$+2\sum_{k=2}^{12}\frac{(\boldsymbol{D}')_{1k}(\boldsymbol{D}')_{k1}}{\lambda_1^2}\frac{1}{1-\lambda_k/\lambda_1}\Big), \tag{11}$$

where $\boldsymbol{B}' = \boldsymbol{V}^{-1}\boldsymbol{B}\boldsymbol{V}$ with matrix elements $B_{ln} = \langle S_{i,1}(l), S_{i,2}(l)|\mathcal{H}_{i,i+1}\mathcal{H}_{i,i+1}\exp(-\beta\mathcal{H}_{i,i+1})|S_{i+1,1}(n), S_{i+1,2}(n)\rangle$, and $\boldsymbol{D}' = \boldsymbol{V}^{-1}\boldsymbol{D}\boldsymbol{V}$ with matrix elements $D_{ln} = \langle S_{i,1}(l), S_{i,2}(l)|\mathcal{H}_{i,i+1}\exp(-\beta\mathcal{H}_{i,i+1})|S_{i+1,1}(n), S_{i+1,2}(n)\rangle$.

3. Results and discussion

In what follows, we focus our attention on a particular case with all antiferromagnetic interactions $J_{||,1} > 0$, $J_{||,2} > 0$, $J_\perp > 0$, and $J_3 > 0$, which yields the most interesting results for the mixed-spin ladder system. J_3 is introduced as a reduced unit for brevity, and then we have $j_{||,1} = J_{||,1}/J_3$, $j_{||,2} = J_{||,2}/J_3$, $j_\perp = J_\perp/J_3$, $h = H/J_3$. In Fig. 2, we present the ground-state phase diagram in the $(j_\perp, h)$ plane. One can see that it demonstrates a variety of spin patterns, and six distinct regions can be identified under the modulation of external field h. The explicit form for each spin configuration and the corresponding energy are listed in Table 1. The ground state in the absence of a magnetic field manifests itself as an antiferromagnetic state AF_1 or AF_2, which is determined by the frustrated parameter $j_\perp$. When $J_\perp/J_3 \leq 2$, the diagonal magnetic bonds with antiferromagnetic arrangement become the ground state AF_1. Otherwise the ground state has the AF_2 configuration with all rung bonds in an antiparallel state. As the magnetic field h increases, various possible magnetization routines are displayed, which summarizes the effects of rung coupling $j_\perp$. It is noteworthy that in this phase diagram, there is a highly-degenerated point ($j_\perp = 0$, $h = 5$) with four ground states emergence, implying the large residual entropy and prominent magnetocaloric effect in this spin chain system under certain conditions.[20–22]

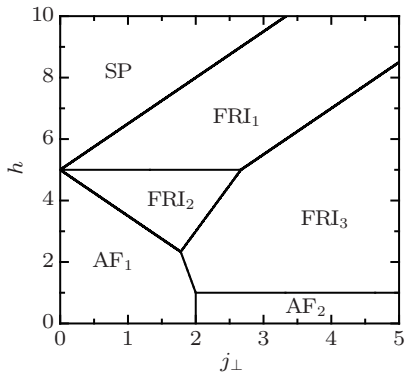


Fig. 2. Ground-state phase diagram in the $j_\perp$–h plane for antiferromagnetic coupling $j_{||,1} = j_{||,2} = 1.0$.

Table 1. Ground states of the system and their energies per block.

Type	Spin configuration	Energy per block
SP	$S_1(3/2, 3/2), S_2(1, 1)$	$\frac{9}{4}J_{\|\|,1} + J_{\|\|,2} + \frac{3}{2}J_\perp + 3J_3 - \frac{5}{2}H$
FRI_1	$S_1(3/2, 3/2), S_2(1, -1)$	$\frac{9}{4}J_{\|\|,1} - J_{\|\|,2} - \frac{3}{2}H$
FRI_2	$S_1(3/2, -3/2), S_2(1, 1)$	$-\frac{9}{4}J_{\|\|,1} + J_{\|\|,2} - H$
FRI_3	$S_1(3/2, 3/2), S_2(-1, -1)$	$\frac{9}{4}J_{\|\|,1} + J_{\|\|,2} - \frac{3}{2}J_\perp - 3J_3 - \frac{1}{2}H$
AF_1	$S_1(3/2, -3/2), S_2(1, -1)$	$-\frac{9}{4}J_{\|\|,1} - J_{\|\|,2} + \frac{3}{2}J_\perp - 3J_3$
AF_2	$S_1(3/2, -3/2), S_2(-1, 1)$	$-\frac{9}{4}J_{\|\|,1} - J_{\|\|,2} - \frac{3}{2}J_\perp + 3J_3$

The diverse zero-temperature spin configuration observed in the phase diagram implies the multiple magnetization plateaus phenomenon and interesting thermodynamic properties. To verify the various indicative fractional plateaus, we perform a detailed examination of the magnetization process. In Fig. 3, we present a three-dimensional (3D) plot of the magnetization as a function of the magnetic field and temperature for two representative rung couplings $j_\perp = 1.0$ and $j_\perp = 2.2$. According to the phase diagram (Fig. 2), one can expect two different sequences of zero-temperature transitions corresponding to $AF_1 \to FRI_2 \to FRI_1 \to SP$ and $AF_2 \to FRI_3 \to FRI_2 \to FRI_1 \to SP$, with possible fractional plateaus at $m/m_s = 1/5$, 2/5, 3/5. As expected, the low-temperature magnetization displays a stepwise profile with a steep increase near the critical field, confirming the transitions just mentioned above, and with temperature increasing, these sharp jumps are gradually rounded off. In addition, it can also be noted that the case of $j_\perp = 2.2$ with the AF_2 ground state is more robust against thermal fluctuations, with magnetization jumps identified up to $t = 0.4$.

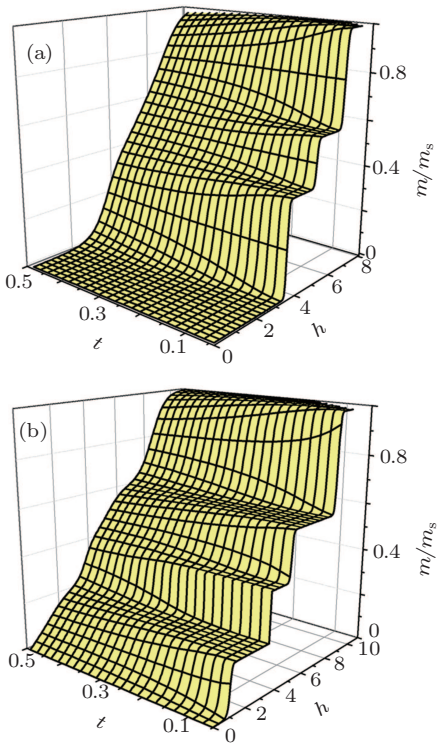


Fig. 3. (color online) 3D plot of the normalized magnetization against temperature and magnetic field for two representative rung couplings (a) $j_\perp = 1.0$ and (b) $j_\perp = 2.2$ under $j_{||,1} = j_{||,2} = 1.0$.

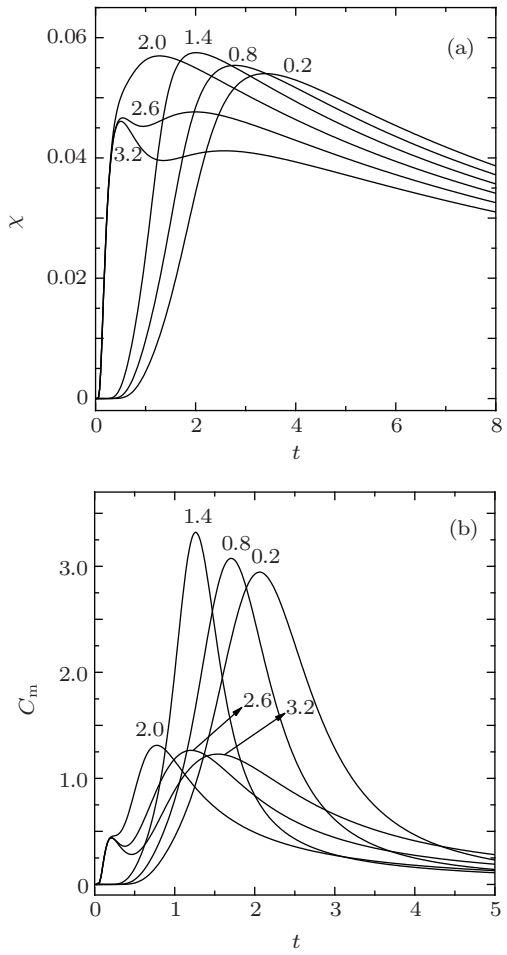


Fig. 4. Temperature dependence of (a) zero-field magnetic susceptibility and (b) zero-field specific heat under $j_{\|,1} = j_{\|,2} = 1.0$ for $j_\perp$ varying from 0.2 to 3.2.

The thermodynamic behaviors of the typical response functions can reveal the competition between ground states AF_1 and AF_2 presented at zero-field. In Fig. 4(a), we report the temperature dependence of zero-field magnetic susceptibility χ for several frustrated parameters $j_\perp$. At $j_\perp = 0.2$, χ starts from zero and reaches its maximum with a broad round peak at intermediate temperature, then gradually vanishes as the temperature approaches zero, exhibiting the main characters of the typical antiferromagnetic correlation. With the enhancement of $j_\perp$, the maximum of χ increases meanwhile shifts towards low temperature region. When $j_\perp = 2.6$, χ presents a double-peak structure. One sharp narrow peak appears at a lower temperature, and a large round peak presents at a relative high temperature. As $j_\perp$ continues to increase, the low-temperature peak almost remains unaffected, but the high-temperature one suffers a significant suppression. In Fig. 4(b), one can observe that the specific heat displays the analogous trend but behaves in a more obvious way. As $j_\perp$ increases from 0.2 to 1.4, the specific heat has a single peak, with its maximum enhanced and shifting towards a low temperature. When $j_\perp$ reaches the critical value 2.0 (the boundary between AF_1 and AF_2 states), an additional second maximum appears in the lower-temperature region, meanwhile the high-temperature larger maximum suffers a great suppression. When $j_\perp$ is further increased, the low-temperature small peak remains in the same status and is unaffected, while the large maximum moves towards the high-temperature region. From the above description, we can deduce that the high-temperature round peak is introduced by thermal excitations between ground-state AF_1 spin configuration and the ones close enough in energy, while the second low-temperature peak most possibly originates from the very strong rung coupling, which drives the system into the AF_2 state.

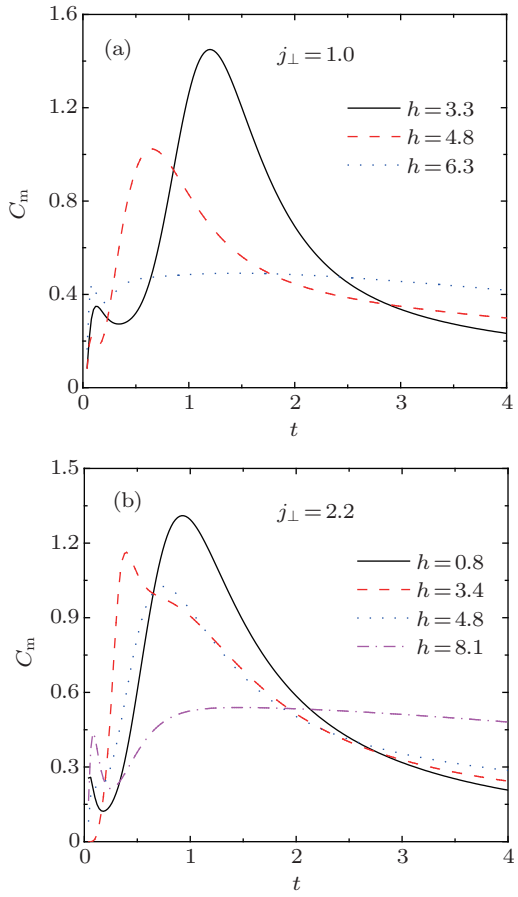


Fig. 5. (color online) Temperature dependence of specific heat for typical rung couplings (a) $j_\perp = 1.0$ and (b) $j_\perp = 2.2$ under several different magnetic fields.

To provide a complete profile of the thermodynamics, in Fig. 5 we plot the thermal variations of the specific heat for $j_\perp = 1.0$ and 2.2 at several external fields which are selected close to the critical values. One can notice that the results become even more interesting with the external magnetic field. In general, the specific heat curve exhibits a double-peak structure, irrespective of the ground state in AF_1 or AF_2. One sharp arises at relative low temperature and around at high temperature. With the enhancement of the magnetic field, both peaks undergo complex changes. For the case shown in Fig. 5(a), one can see that the low-temperature peak suffers a suppression at first, and then strengthens, meanwhile moving back and forth along the temperature axis. In comparison, the overall trend of

the high-temperature peak is very regular, with its maximum dropping in magnitude and shifting towards lower temperatures. Especially when the field ($h = 6.3$) is near the FRI_1–SP border, it becomes quite broad and flat, with almost the same height of that of the low-temperature one. The specific heat of the other typical case $j_\perp = 2.2$ in Fig. 5(b) shows the similar features, except the profile close to the FRI_2–FRI_1 border with $h = 3.4$. In that exceptional circumstance, we notice that the low-temperature peak receives remarkable enhancement even beyond the high-temperature round one. If we consult to the ground-state phase diagram, it is not difficult to find that all these thermal variations in essence are reflections of different ground-states transitions driven by external field and temperature.

4. Conclusion

The two-leg mixed spin-$(3/2, 1)$ ladder with frustrated rung coupling and next-nearest-neighbor interaction has been investigated in detail in this paper. The transfer-matrix method is employed to obtain the exact solutions of the basic thermodynamic quantities for the simplified version Ising-chain model. Based on the analytical results, we particularly examine the ground state, magnetization process, thermal variations of magnetic susceptibility and specific heat. Six different spin configurations can be identified in the phase diagram under the interplay between the external field and frustrated interactions. Meanwhile, the multiple plateau behavior is also evidently detected in the magnetization plots, showing an excellent coincidence with the information provided by the phase diagram. Furthermore, we also discuss the impacts of frustrated rung coupling and external field on the thermodynamic properties of this exactly solved model. It is shown that strong rung coupling will bring in an additional low-temperature peak in the zero-field magnetic susceptibility and specific heat curves. The application of external field will generate a complex variation on the double-peak structure of specific heat, implying the inherent property of different zero-temperature phase transitions.

References

[1] Wang X 2000 *Mod. Phys. Lett. B* **14** 327
[2] Liu G H, Wang H L and Tian G S 2008 *Phys. Rev. B* **77** 214418
[3] Kohama Y 2012 *Phys. Rev. Lett.* **109** 167204
[4] Shi D 2010 *Chin. Phys. B* **19** 077503
[5] Herringer S N 2014 *Chem. Eur. J.* **20** 8355
[6] Rüegg Ch 2008 *Phys. Rev. Lett.* **101** 247202
[7] Li Y C and Lin H Q 2012 *New J. Phys.* **14** 063019
[8] Allen P, Azaria P and Lecheminant P 2001 *J. Phys. A: Math. Gen.* **34** L305
[9] Zheng W, Kotov V and Oitmaa J 1998 *Phys. Rev. B* **57** 11439
[10] Arčon D 1999 *Phys. Rev. B* **60** 4191
[11] Sorai M 2013 *Chem. Rev.* **113** PR41
[12] Hagiwara M 1998 *J. Phys. Soc. Jpn.* **67** 2209
[13] Lou J, Chen C and Qin S 2001 *Phys. Rev. B* **64** 144403
[14] Ivanov N B and Richter J 2006 *Phys. Rev. B* **73** 132407
[15] Chandra V R, Ivanov N B and Richter J 2010 *Phys. Rev. B* **81** 024409
[16] Qiao J and Zhou B 2015 *Chin. Phys. B* **24** 110306
[17] Kiššová J and Strečka J 2008 *Acta Phys. Pol. A* **113** 445
[18] Lisnii B M 2011 *Low Temp. Phys.* **37** 296
[19] Jozef S, Lucia C and Kazuhiko M 2009 *Phys. Rev. E* **79** 051103
[20] Pereira M S S, de Moura F A B F and Lyra M L 2009 *Phys. Rev. B* **79** 054427
[21] Ohanyan V and Honecker A 2012 *Phys. Rev. B* **86** 054412
[22] Strečka J 2014 *Phys. Rev. E* **89** 022143